It was found that the contribution of the long-range fluctuation to the total fluctuation $\gamma(r)$ is usually very small, ranging around a few per cent, and that a_2, which reaches $\sim 1\ \mu$, is much larger than a_1 varying from several hundred to a few thousand ångströms with good correlation to the size of the dispersed spheres.

Three kinds of heterogeneity parameters, "specific surface" S_{sp}, "distance of heterogeneity" $\bar{l}_c$, and "volume of heterogeneity" $\bar{v}$, which were further defined from the correlation function $\gamma(r)$, as well as the statistical parameters, such as a_1 and a_2, and the fractional contribution factors of the short- and long-range fluctuations, f and $(1 - f)$, were discussed in relation to the heterogeneity of the colloidal domain structures of the specimens observed from their electron micrographs.

The following conclusions were obtained. The larger the size of the spherical domain, the larger the correlation distances, a_1 and a_2, as well as the heterogeneity parameters, $\bar{l}_c$ and $\bar{v}$, and, in contrast, the smaller the specific surface S_{sp}. The larger the distance between the dispersed spherical domains, the larger the long-range correlation distance. The less uniform the dispersion of the spherical domains, the larger the short-range correlation distance a_1 as well as the heterogeneity parameters, $\bar{l}_c$ and $\bar{v}$, and, in contrast, the smaller the long-range correlation distance a_2 and the fractional contribution factor of the long-range fluctuation $(1 - f)$. The radius of the dispersed spheres R_{scatt}, which is determined from the parameter S_{sp}, agrees fairly well with $R_{E.M.}$ determined from the electron micrograph of the domain structures.

Acknowledgments. The authors are deeply indebted to Dr. K. Kato and Mr. M. Nishimura, Central Research Laboratory, Toyo Rayon Co. Ltd., for kindly arranging for preparation of the electron micrographs.

A part of this work was supported by the grant from the Scientific Research Funds (Kagaku Kenkyu-hi, 19214-1967) of the Ministry of Education, Japan, and the grant from the Japan Synthetic Rubber Co. Ltd., Tokyo, Japan.

Structure of Isotactic Poly(methyl methacrylate)

Hiroyuki Tadokoro, Yôzô Chatani, Hiroshi Kusanagi, and Masaaki Yokoyama

Department of Polymer Science, Faculty of Science, Osaka University, Toyonaka, Osaka, Japan. *Received March 16, 1970*

ABSTRACT: The structure of isotactic poly(methyl methacrylate) in the crystalline state was analyzed by the use of X-ray diffraction and far-infrared spectroscopic methods. At the first stage, the results of the conformational analysis, cylindrical Patterson function, and molecular structure factor calculation have led two types of helix models, of which the main difference lies in the conformation of the side chain. For both models the main chain is composed of a (5/1) helix containing five chemical units and one turn in the fiber identity period (the internal rotation angles; $\tau_1 = 180°$ and $\tau_2 = -108°$). Finally, one of these models has been found to be more reasonable from the far-infrared spectroscopy and normal coordinate treatment. The internal rotation angles of the side chain for this model are $\tau_3 = -24°$ and $\tau_4 = 171°$ in CH_3–C_{τ_3}–CO_{τ_4}–O–CH_3 and the α-CH_3 group points outward from the helix.

Poly(methyl methacrylate) (PMMA) can be prepared as samples from highly isotactic to syndiotactic depending upon the polymerization condition. This polymer has been noted for its importance from the viewpoint of nmr spectroscopy and mechanism of polymerization. The configuration, *i.e.*, isotactic or syndiotactic, was determined by nmr by noticing the absorption of methylene protons.[1,2]

The molecular conformation or crystal structure, however, has not yet been settled. Stroupe and Hughes[3] proposed a (5/2) helix model for isotactic PMMA. Here (5/2) denotes a helix which contains five chemical units and turns twice in the fiber identity period. Liquori and his coworkers[4] studied the ultraviolet spectrum of a dioxane solution of isotactic PMMA at various temperatures, and from this result and also from conformational analysis they suggested that the chain transforms from (5/1) to (5/2) helix at 43°. Furthermore, Liquori, *et al.*,[5] reported the formation of a crystalline complex of syndiotactic PMMA and isotactic PMMA with the mole ratio of 2:1.

In their article they noted that the Fourier transform of (5/2) helix was found to be inconsistent with the intensity distribution of the fiber photograph of isotactic PMMA; however, they have not reported further detailed results.

We have studied the structure of isotactic PMMA by the use of X-ray diffraction and far-infrared spectroscopy. From the results of the conformational analysis, cylindrical Patterson function, and molecular structure factor calculation, the possible models have been restricted to two types of (5/1) helices, one of which was finally found to be more reasonable from the far-infrared spectroscopic method.

(1) F. A. Bovey and G. V. D. Tiers, *J. Polym. Sci.*, **44**, 173 (1960).

(2) A. Nishioka, H. Watanabe, K. Abe, and Y. Sono, *ibid.*, **48**, 241 (1960).

(3) J. D. Stroupe and R. E. Hughes, *J. Amer. Chem. Soc.*, **80**, 2341 (1958).

(4) M. D'alagni, P. De Santis, A. M. Liquori, and M. Savino, *J. Polym. Sci., Part B*, **2**, 925 (1964).

(5) A. M. Liquori, Q. Anzuino, V. M. Coiro, M. D'alagni, P. De Santis, and M. Savino, *Nature (London)*, **206**, 358 (1965).

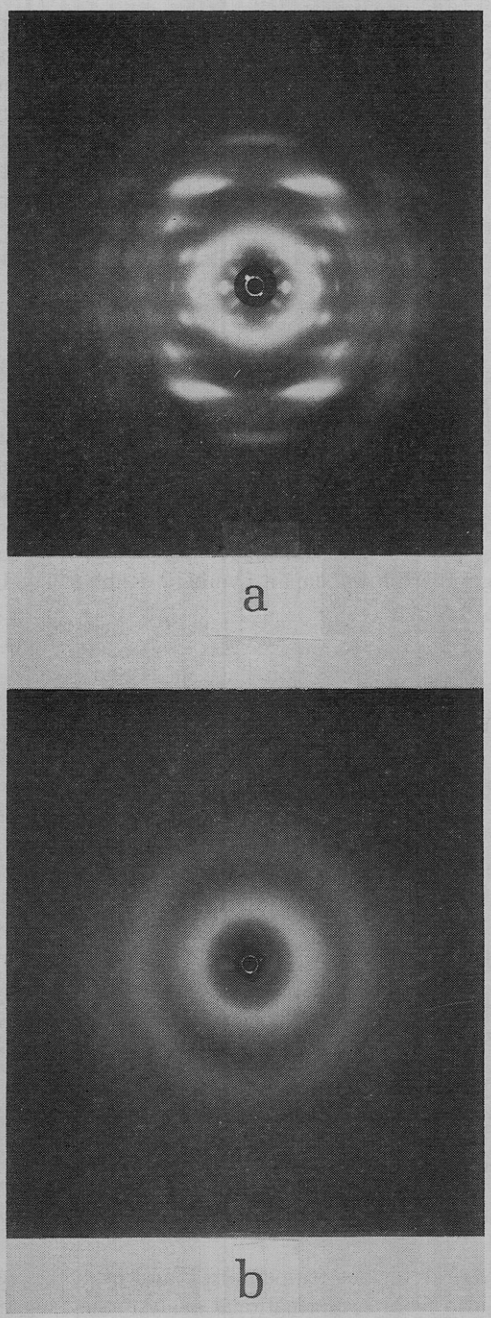

Figure 1. X-Ray fiber photographs of (a) isotactic PMMA and (b) syndiotactic PMMA.

Experimental Section

Samples. The following samples were used in the present studies: (1) isotactic PMMA, the tactic index I (triad) measured by nmr is about 100%; (2) syndiotactic PMMA, the triad index S is about 94%. Both these samples were kindly supplied by Dr. Y. Kotake of the Research Laboratory, Mitsubishi Rayon Co., Ltd.

X-Ray Diffraction and Infrared Absorption Measurements. The films of isotactic PMMA for X-ray and infrared measurements were prepared by casting from toluene solution, stretching to about five to ten times the original lengths, and subsequently heat treating at 90° for 6 hr under vacuum. The X-ray diffraction measurements were made with Ni-filtered Cu Kα radiation by using a cylindrical camera. The isotactic sample gave an oriented crystalline X-ray pattern as shown in Figure 1a.

The far-infrared spectra were measured with a Hitachi Model FIS-1 double-beam far-infrared grating spectrophotometer with polarizer of polyethylene sheets. The polarized far-infrared spectra of isotactic PMMA are shown in Figure 2. The solid and broken curves represent the absorptions obtained with polarized radiation with the electric vector perpendicular and parallel to the orientation direction, respectively. The figures adjacent to the curves represent the specimen thickness in microns measured by a bench thickness gauge.

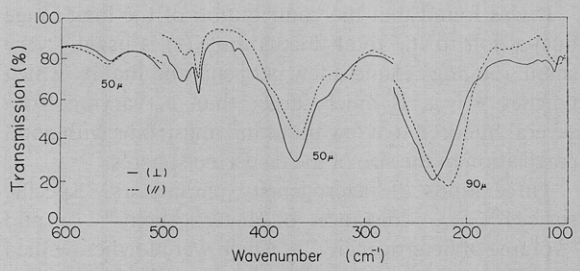

Figure 2. Far-infrared spectra of isotactic PMMA (600–80-cm^{-1} region). The solid and broken curves represent the spectra measured by the polarized radiation with the electric vector perpendicular and parallel to the fiber axis, respectively. The band at 464 cm^{-1} is due to toluene.

Analysis

Since syndiotactic PMMA gave the X-ray pattern of very low crystallinity (Figure 1b), the analysis has been made exclusively on isotactic PMMA. The outline of the process of analysis is schematically shown in Figure 3. The fiber photograph of isotactic PMMA is approximately indexed with an orthorhombic unit cell with lattice constants a = 21.08 Å, b = 12.17 Å, and c(fiber axis) = 10.50 Å, as already reported by Stroupe and Hughes.[3] Because of the broadness of the reflections, the exact indexing is rather difficult and the space group could not be determined. Since the general feature of the fiber photograph suggests a helical structure containing five chemical units in the fiber identity period, the molecular conformation can be given, if the four kinds of internal rotation angles are determined:

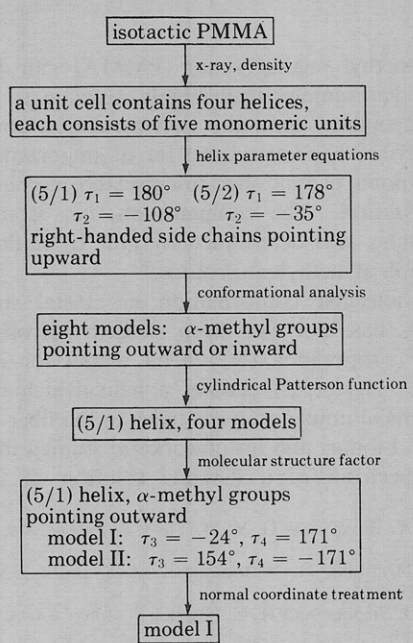

Figure 3. Process of analysis.

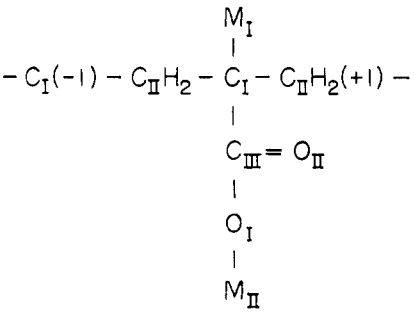

Figure 4. Numbering of the atoms.

$\tau_1[C_{II}(-1)C_I(-1)C_{II}C_I]$, $\tau_2[C_I(-1)C_{II}C_IC_{II}(+1)]$, τ_3-$[M_IC_IC_{III}O_I]$, and $\tau_4[C_IC_{III}O_IM_{II}]$. The numbering of the atoms is shown in Figure 4.

The bond lengths and bond angles used throughout this investigation are as follows: bond lengths, C_{II}–H = 1.10 Å, C_{II}–C_I = C_I–$C_{II}(+1)$ = C_I–M_I = C_I–C_{III} = 1.54 Å, C_{III}–O_{II} = 1.21 Å, C_{III}–O_I = 1.32 Å, O_I–M_{II} = 1.46 Å; bond angles, $C_IC_{II}(+1)C_I$-$(+1)$ = $C_{III}O_IM_{II}$ = 114°, $O_IC_{III}O_{II}$ = 124°, C_I-$C_{III}O_{II}$ = 120°, $C_IC_{III}O_I$ = 116°, and other bond angles = 109°28′.

Molecular Models. At first the internal rotation angles τ_1 and τ_2 of the skeletal chain were examined by using the helical parameter equation proposed by Miyazawa[6] by assuming that five monomeric units are contained in the fiber identity period of 10.50 Å. From this result two following helical models were found to be suitable: (5/1) helix with τ_1 = 180° and τ_2 = −108°, and (5/2) helix with τ_1 = 178° and τ_2 = −35°. The sign of the angle, *e.g.*, τ_1, is positive if, viewing the atoms along the bond $C_I(-1)$–C_{II} with $C_I(-1)$ nearer the observer than C_{II}, the angle from the projection of C_I-(-1)–$C_{II}(-1)$ to the projection of C_{II}–C_I is traced in the clockwise sense as usual. Hereafter we consider only right-handed helices with the side chains pointing upward for simplicity.

There remained two internal rotation angles of the side chain τ_3 and τ_4 undetermined, which were examined by conformational analysis. The method of analysis is essentially the same as those reported by De Santis, *et al.*,[7] and Scott and Scheraga.[8] The potential functions between nonbonded atoms used here are the Lennard-Jones type 6–12 function with the same parameters used by Scott and Scheraga[9] except the methyl group, which were considered as a united atom. The additivity was assumed for the polarizability α and for the effective number of the outer shell electrons N. Thus for CH_3 group, $\alpha(C) + \alpha(H) \times 3$ = 0.93 Å^3 + 0.42 Å^3 × 3 = 2.19 Å^3, and $N(C) + N(H) \times 3$ = 5.2 + 0.9 × 3 = 7.9. A van der Waals radius of CH_3 = 2.0 Å was used. The potential energies were calculated for all the atom pairs of the distance shorter than 5 Å, actually between the atoms belonging to second neighboring units. The dipole interactions were not taken into account.

(6) T. Miyazawa, *J. Polym. Sci.*, **55**, 215 (1961).
(7) P. De Santis, E. Giglio, A. M. Liquori, and A. Ripamonti, *ibid., Part A*, **1**, 1383 (1963).
(8) R. A. Scott and H. A. Scheraga, *J. Chem. Phys.*, **44**, 3054 (1966).
(9) R. A. Scott and H. A. Scheraga, *ibid.*, **45**, 2091 (1966).

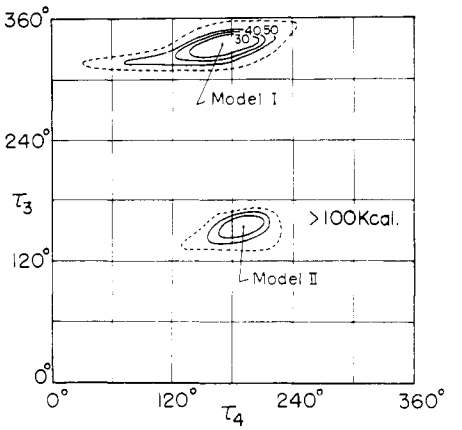

Figure 5. Potential energy map for the (5/1) helix with the α-CH_3 group pointing outward. The broken curves indicate the contour for 100 kcal/mol monomeric unit. The upper minimum with 29 kcal and the lower one with 32 kcal correspond to model I and model II, respectively.

There are two possibilities for determining whether the α-CH_3 groups point to the outside or inside of the helix for both the (5/1) and (5/2) helices, so four kinds of potential maps should be prepared. One of these is shown in Figure 5, which is for the (5/1) helix with the α-CH_3 groups pointing outward. The potential contours were drawn for τ_3 (ordinate) and τ_4 (abscissa). Two minima were found at τ_3 = 336° (= −24°) and τ_4 = 171° with the potential value 29 kcal/mol monomeric unit (we denoted this model as model I), and τ_3 = 154° and τ_4 = 189° (= −171°) with 32 kcal/mol monomeric unit (model II). Thus four models were found for each of the (5/1) and (5/2) helices, a total of eight models.

Cylindrical Patterson Function. For deciding whether the (5/1) or (5/2) helix is reasonable, the cylindrical Patterson function $\phi(z,r)$[10,11] was utilized

$$\phi(z,r) = \frac{1}{NV}\sum_l\sum_\xi I(l,\xi)J_0(2\pi\xi r)\cos(2\pi lz/c) \quad (1)$$

Here z and r are the distance in the fiber direction and the distance from the fiber axis on the cylindrical coordinate in the Patterson space, respectively. ξ is the Bernal coordinate; $I(l,\xi)$ is the integrated intensity of a reflection of the lth layer line at a distance ξ; V is the volume irradiated; and N is the total number of periods in the fiber direction; $J_0(2\pi\xi r)$ is the Bessel function of zero order.

Figure 6(a) is the cylindrical Patterson map calculated by using the observed intensity of 48 independent reflections. It is a characteristic feature of this map that there appears a maximum at the origin and a minimum at the point $z = c/2$ and $r = 0$. This feature suggests that the distance between a turn and succeeding turn along the axis corresponds to the fiber period, that is, the (5/1) helix is reasonable.

The Patterson function synthesized by using the molecular structure factors calculated for the (5/1) helix (model I) and the (5/2) helix (a model with the conforma-

(10) C. H. MacGillavry and E. M. Bruins, *Acta Crystallogr.*, **1**, 156 (1948).
(11) R. E. Franklin and R. G. Gosling, *ibid.*, **6**, 678 (1953).

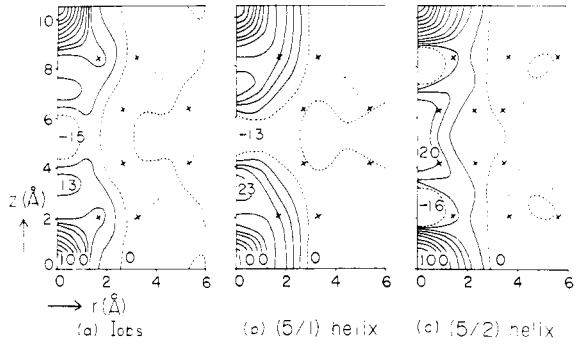

Figure 6. Cylindrical Patterson maps synthesized from (a) the observed intensity, (b) and (c) the molecular structure factors calculated for (5/1) helix and (5/2) helix, respectively: ×, theoretical peaks for intrahelical CH_3–CH_3 (in the ester group) and C–C (in the skeletal chain) vectors.

tion of the side chain similar to model I) instead of the observed values is shown for comparison in Figures 6(b) and (c), respectively. The result from the observed reflection data is in far better agreement with the map for the (5/1) model than the map for the (5/2) helix, which has a maximum at $z = c/2$ and $r = 0$. Thus the (5/2) helix model was excluded.

Molecular Structure Factor. Now we should examine the most reasonable of the four models of the (5/1) helices. The intensity diffracted by a lattice containing one helical molecule at the lattice point can be calculated from the squares of the following Fourier transform derived by Cochran, Crick, and Vand[12]

$$F(R,\psi,l/c) = \sum_n \sum_j f_j J_n(2\pi R r_j) \exp[i(n\psi - n\phi_j + n\pi/2 + 2\pi l z_j/c)] \quad (2)$$

where R, ψ, and l/c are cylindrical coordinates of a point in reciprocal space, f_j is the atomic structure factor, and r_j, ϕ_j, and z_j are cylindrical coordinates of the jth atom. J_n is Bessel function, the order n of which is obtained for the reflections on the lth layer line by solving the following equation for the (5/1) helix

$$l = n + 5m \quad (3)$$

where m is an integer.

Since in the present case four chains pass through a unit cell, the phase relation between the X-rays scattered by the chains in the unit cell should be taken into account for the calculation of the structure factor. At present, however, the space group of isotactic PMMA has not yet been determined, and it is difficult to assume the values of the parameters locating the helical chains in the unit cell as well as the senses of rotation and direction (upward or downward) of the molecules. In the present work, therefore, the phase relation was not taken into account for the first approximation. In the fiber photograph the relevant intensity should be cylindrically averaged, which can be expressed as[13]

$$\langle F^2(R,l/c)\rangle_\psi = \sum_n \{[\sum_j f_j J_n(2\pi R r_j) \cos(2\pi l z_j/c - n\phi_j)]^2 + [\sum_j f_j J_n(2\pi R r_j) \sin(2\pi l z_j/c - n\phi_j)]^2\} \quad (4)$$

Figure 7 shows the calculated intensities [$\langle F^2(R,l/c)\rangle_\psi$ of eq 4] for the four models. The vertical rods in the figure show the observed relative intensities of the reflections after corrected by Lorentz and polarization factors. In the figure the curves on the left-hand side (a) are for the models with the α-CH_3 pointing outward from the helix (solid line, model I; broken line, model II), and the curves on the right-hand side (b) are for the two models with the α-CH_3 pointing inside toward the helix. The values of the observed intensity show better agreement with the calculated values for the models with the α-CH_3 pointing outward (model I and model II) than those for the models with the α-CH_3 pointing inside. Thus models I and II were found to be the most reasonable among the eight models assumed at the first stage, but the determination of the final model was still difficult from the present X-ray data alone.

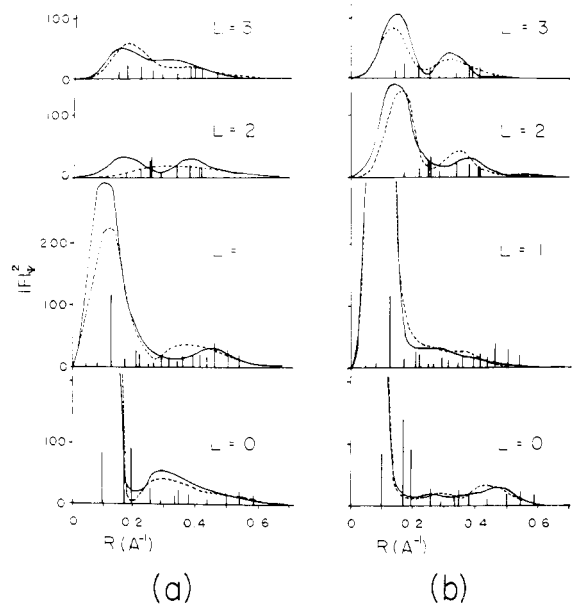

Figure 7. Comparison between the observed relative intensities (vertical rods) and the calculated molecular structure factors (a) for the two models with the α-CH_3 pointing outward (solid curves, model I; broken curves, model II), and (b) for the two models with the α-CH_3 pointing inside.

Far-Infrared Spectra and Normal Coordinate Treatment. It may be expected that the difference between the conformations of model I and model II is reflected in the far-infrared spectra. In order to make the normal coordinate treatment, a well-established set of force constants is necessary especially for the ester group. We have studied the far-infrared spectra of a series of aliphatic polyesters $[-(CH_2)_mCOO-]_n$ (m = 1, 2, 4, and 5), and found several far-infrared bands appearing systematically at nearly the same positions with similar intensities.[14] On the other hand the conformations of these polyesters were found to be essentially planar zigzag by X-ray studies.[15-17] We have

(12) W. Cochran, F. H. C. Crick, and V. Vand, *Acta Crystallogr.*, **5**, 581 (1952).
(13) D. R. Davies and A. Rich, *ibid.*, **12**, 97 (1957).
(14) H. Tadokoro, M. Kobayashi, H. Yoshidome, K. Tai, and D. Makino, *J. Chem. Phys.*, **49**, 3359 (1968).
(15) Y. Chatani, K. Suehiro, Y. Okita, H. Tadokoro, and K. Chujo, *Makromol. Chem.*, **133**, 215 (1968).
(16) K. Suehiro, Y. Chatani, H. Tadokoro, R. Kato, and A. Tanaka, Annual Meeting of Society of Polymer Science (Japan), Nagoya, Japan, May 1966.
(17) Y. Okita, Y. Chatani, H. Tadokoro, and Y. Yamashita, Annual Meeting of Society of Polymer Science (Japan), Tokyo, Japan, May 1967.

TABLE I
CHARACTER TABLE, NUMBER OF NORMAL MODES, AND SELECTION RULES FOR ISOTACTIC PMMA UNDER THE POINT GROUP C_5[a]

C_5	E	C_5	C_5^2	C_5^3	C_5^4	N_i[b]	Ir	Raman[c]
A	1	1	1	1	1	$21 - 2(T_z,R_z)$	A(∥)	A
E_1	1	ϵ	ϵ^2	ϵ^{2*}	ϵ^*	$[21 - 1(T_z \text{ or } T_y)] \times 2$	A(⊥)	A
	1	ϵ^*	ϵ^{2*}	ϵ^2	ϵ			
E_2	1	ϵ^2	ϵ^*	ϵ	ϵ^{2*}	$[21] \times 2$	F	A
	1	ϵ^{2*}	ϵ	ϵ^*	ϵ^2			

[a] $\epsilon = \exp(2\pi i/5)$. [b] N_i, the number of normal modes. T and R are translation and rotation of a molecule as a whole. [c] A, active; F, forbidden.

calculated the normal vibrations of the skeleton of these polyesters, and found a reasonable set of force constants.[14]

The normal coordinate treatments of models I and II were carried out according to the same method that was applied in previous investigations.[14] The methyl and methylene groups were considered as united atoms with the atomic weights of CH_3 and CH_2, respectively. The fundamental vibrations of the (5/1) helix infinitely extended may be treated under the factor group isomorphous to the point group C_5. The result of the factor group analysis for the skeletal model is given in Table I. The totally symmetric A species gives rise to 19 fundamental modes which have the transition moments parallel to the helical axis, and the doubly degenerate E_1 species gives 20 doubly degenerate fundamentals with the transition moments perpendicular to the helical axis. The normal modes of these two symmetry species as well as the E_2 modes are all Raman active.

The force constants of the modified Urey–Bradley type were directly transferred from those obtained for the aliphatic polyesters[14] as shown in Table II. The normal frequencies and potential energy distributions calculated for models I and II are compared with the observed data in Table III. The bands of the frequencies higher than 700 cm^{-1} are omitted from this table for simplicity, since the skeletal vibrations are in question in the present study. It is empirically well known that the normal vibrations including internal coordinates such as δ(CCO), δ(OC=O), and δ(COC) give rise to comparatively strong bands in the infrared spectra. The calculated modes should be assigned to the observed bands with due regard to the potential energy distributions in addition to the calculated frequencies. Then, in the case of model I the calculated frequencies, 365 cm^{-1} (E_1) and 368 cm^{-1} (A), may be assigned to the observed strong bands at 368 cm^{-1} (perpendicular) and 365 cm^{-1} (parallel), respectively, since the potential energy distributions of these calculated modes are mainly composed of the deformation $\delta(C_{III}O_IM_{II})$ for both species (potential energy distribution, 59% for the A species and 55% for the E_1 species). This assignment also seems to be reasonable from the results of the previous study on the aliphatic polyesters.[14] On the other hand, in the case of model II the modes having the calculated frequencies, 369 cm^{-1} (E_1) and 385 cm^{-1} (A), should not be assigned to these two observed bands, though the calculated frequencies are close to them. The potential energy distributions of these modes are mainly of the deformation $\delta(C_IM_I)$ for both species (36% for the A species and 40% for the E_1 species). The calculated frequencies for model II with the vibrational modes similar to the calculated modes for model I at 365 cm^{-1} (E_1) and 368 cm^{-1} (A) are 399 cm^{-1} (E_1) and 390 cm^{-1} (A), respectively. It may be rather reasonable to assign them to the observed bands

TABLE II
FORCE CONSTANTS FOR ISOTACTIC PMMA[a]

$K(C_{II}C_I)$, $K(C_IC_{II}(+1))$	3.90[c]
$K(O_IM_{II})$	3.80[c]
$K(C_IM_I)$	3.90[c]
$K(C_IC_{III})$	2.80[c]
$K(O_IC_{III})$	2.90[c]
$K(C_{III}O_{II})$	10.70[c]
$H(C_{II}C_IC_{II}(+1))$	0.310[c]
$H(C_I(-1)C_{II}C_I)$	0.310[c]
$H(C_{II}C_IM_I)$	0.310[c]
$H(C_{II}C_IC_{III})$	0.350[c]
$H(M_IC_IC_{III})$	0.350[c]
$H(M_{II}O_IC_{III})$	0.610[c]
$H(C_IC_{III}O_{II})$	0.570[c]
$H(O_IC_{III}O_{II})$	0.300[c]
$H(C_IC_{III}O_I)$	0.320[c]
$H_\tau(C_I(-1)C_{II}-C_IC_{II}(+1))$, $H_\tau(C_{II}C_I-C_{II}(+1)C_I(+1))$	0.099[d]
$H_\tau(M_IC_I-C_{III}O_{II})$	0.134[d]
$H_\tau(M_IC_I-C_{III}O_I)$	0.093[d]
$H_\tau(M_{II}O_I-C_{III}O_{II})$	0.279[d]
$H_\tau(M_{II}O_I-C_{III}C_I)$	0.110[d]
$F(C_{II}C_IC_{II}(+1))$	0.525[c]
$F(C_I(-1)C_{II}C_I)$	0.525[c]
$F(C_{II}C_IM_I)$	0.525[c]
$F(C_{II}C_IC_{III})$	0.500[c]
$F(M_IC_IC_{III})$	0.500[c]
$F(C_IC_{III}O_{II})$	0.530[c]
$F(O_IC_{III}O_{II})$	1.750[c]
$F(C_IC_{III}O_I)$	0.640[c]
$F(M_{II}O_IC_{III})$	0.390[c]
F'	$-0.1F$[c]
$C[\delta(C_IC_{III}O_{II})-\delta(C_{III}C_IC_{II}(+1))]$ for model I, $C[\delta(C_IC_{III}O_{II})-\delta(C_{III}C_IM_I)]$ for model II	0.24[d]
$C[\delta(M_{II}O_IC_{III})-\delta(O_IC_{III}O_{II})]$	0.20[d]
$\chi[\tau(M_IC_IC_{III}O_I)-\tau(M_IC_IC_{III}O_{II})]$	-0.060[d]
$\chi[\tau(M_{II}O_IC_{III}C_I)-\tau(M_{II}O_IC_{III}O_I)]$	-0.044[d]

[a] K, H, H_τ, and F are the stretching, bending, torsional, and repulsive force constants; C, χ are coupling constants between the internal coordinates. [b] The *cis*-coupling constants are taken differently for the two models because of the different conformation of the side chain in the two models. [c] Units are mdyn/Å. [d] Units are mdyn Å.

TABLE III
SKELETAL VIBRATIONS OF ISOTACTIC PMMA

Obsd freq, cm^{-1}	Model I: Calcd freq, cm^{-1}	Model I: Assignment[a] potential energy distribution	Model II: Calcd freq, cm^{-1}	Model II: Assignment[a] potential energy distribution
		Species A		
	685	$\gamma(C_{III}{=}O_{II})$ (40) − $w(C_IC_{III})$ (26)	693	$\gamma(C_{III}{=}O_{II})$ (41) + $w(C_IC_{III})$ (25)
568(∥) vw (sh)	635	$\delta(C_{II}C_IC_{II}(+1))$ (29) − $\nu(C_IM_I)$ (20)	612	$\delta(C_{II}C_IC_{II}(+1))$ (17) − $\delta(C_{III}{=}O_{II})$ (17)
559(∥) m	555	$w(C_IM_I)$ (36)	600	$\delta(C_{II}C_IC_{II}(+1))$ (26)
476(∥) m	457	$\delta(C_IM_I)$ (28) + $\delta(C_{III}{=}O_{II})$ (22)	414	$w(C_IM_I)$ (43)
391(∥) w (sh)	390	$w(C_IM_I)$ (43) + $\delta(C_{II}C_IC_{II}(+1))$ (21)		
365(∥) vs	368	$\delta(C_{III}O_IM_{II})$ (59)	390	$\delta(C_{III}O_IM_{II})$ (50)
			385	$\delta(C_IM_I)$ (36)
314(∥) m	280	$\tau(C_{III}O_I)$ (28) + $w(C_IC_{III})$ (27)	264	$\delta(C_IC_{III}O_I)$ (37) − $\delta(C_{III}O_IM_{II})$ (20)
217(∥) s	231	$\delta(C_IC_{III}O_I)$ (36) + $\delta(C_IM_I)$ (26)	254	$w(C_IC_{III})$ (31) − $\delta(C_IM_I)$ (20)
165(∥) vw (b)	161	$\tau(C_{III}O_I)$ (36)	157	$\tau(C_{III}O_I)$ (31) − $\gamma(C_{III}{=}O_{II})$ (22)
109(∥) m	91	$\tau(C_IC_{III})$ (31)	81	$\tau(C_IC_{III})$ (36)
		Species E_1		
675(⊥) vw	709	$\gamma(C_{III}{=}O_{II})$ (31, 79°), $w(C_IC_{III})$ (27, 260°)	724	$\gamma(C_{III}{=}O_{II})$ (28, −30°), $w(C_IC_{III})$ (25, −27°)
609(⊥) vw	655	$\delta(C_{III}{=}O_{II})$ (23)	658	$\delta(C_{III}{=}O_{II})$ (24, −48°), $\delta(C_IM_I)$ (20, 145°)
559(⊥) m	593	$w(C_IM_I)$ (31)	579	$\delta(C_{II}C_IC_{II}(+1))$ (30, 140°), $w(C_IM_I)$ (26, 224°)
480(⊥) m	502	$\delta(C_{II}C_IC_{II}(+1))$ (15, 31°), $\delta(C_IM_I)$ (14, −78°)	520	$\delta(C_IC_{III})$ (11, 166°), $\delta(C_{III}{=}O_{II})$ (10, −76°)
406(⊥) w (sh)	436	$\delta(C_{III}{=}O_{II})$ (21)		
368(⊥) vs	365	$\delta(C_{III}O_IM_{II})$ (55, −55°), $\delta(C_IM_I)$ (23, −53°)	399	$\delta(C_{III}O_IM_{II})$ (32, 172°), $\delta(C_{III}{=}O_{II})$ (20, −9°)
			369	$\delta(C_IM_I)$ (40)
338(⊥) m (sh)	281	$w(C_IM_I)$ (20, 153°), $\delta(C_IC_{III}O_I)$ (20, 210°)	301	$\delta(C_{III}O_IM_{II})$ (27)
232(⊥) s	230	$\delta(C_IC_{III})$ (19, 94°), δ $(C_IC_{III}O_I)$ (18, −23°)	242	$w(C_IM_I)$ (30)
188(⊥) vw	201	$\delta(C_IC_{III})$ (14, 231°), $\delta(C_{II}C_IC_{II}(+1))$ (14, 157°)	188	$\tau(C_{III}O_I)$ (24, 6°), $\delta(C_IC_{II}C_I(+1))$ (15, −66°)
140(⊥) vw (b)	154	$\tau(C_{III}O_I)$ (37)	151	$\tau(C_{III}O_I)$ (26, 209°), $\delta(C_IC_{III})$ (16, 246°)
113(⊥) w	75	$\tau(C_IC_{III})$ (43)	70	$\tau(C_IC_{III})$ (40)

[a] δ, bending; w, wagging; τ, torsion; ν, stretching; $\delta(C_{III}{=}O_{II})$, carbonyl in-plane bending; $\gamma(C_{III}{=}O_{II})$, carbonyl out-of-plane bending. The potential energy distribution (in per cent) among the symmetry coordinates is given in parentheses. The signs for the A species and the degrees of angle in parentheses for the E_1 species denote the phase relations of the coupled coordinates, respectively.

at 368 and 365 cm^{-1} in spite of the significant difference between observed and calculated frequencies. It can be seen in Table III that the modes with the calculated frequencies, 230 cm^{-1} (E_1) and 231 cm^{-1} (A) for model I, assigned to the other observed strong bands at 232 cm^{-1} (perpendicular) and 217 cm^{-1} (parallel), respectively, consist of the deformation $\delta(C_IC_{III}O_I)$. In the case of model II, however, the calculated frequencies closest to these strong bands are 242 cm^{-1} (E_1) and 254 cm^{-1} (A), and these calculated modes have rather complicated potential energy distributions mainly including $w(C_IC_{III})$, $\delta(C_IM_I)$, and $w(C_IM_I)$. The potential energy distributions for model I explain the relative intensity of the infrared spectra of isotactic PMMA far more satisfactorily than those for model II.

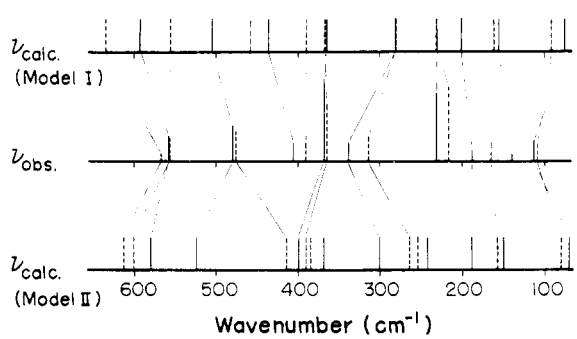

Figure 8. The observed frequencies (middle) and calculated frequencies for model I (top) and model II (bottom). The solid and broken rods indicate the perpendicular and parallel bands, respectively. The thin lines give the assignment of the calculated modes.

It should be also noticed that two bands at 480 cm^{-1} (perpendicular) and 476 cm^{-1} (parallel) appear at frequencies close to each other. Model I gives the corresponding calculated frequencies, 502 cm^{-1} (E_1) and 457 cm^{-1} (A), respectively, the difference of which is rather small, and they are in good agreement with the observed data. On the contrary, model II gives 520 cm^{-1} (E_1) and 414 cm^{-1} (A), which are too far apart from each other in comparison with the observed frequencies.

In Figure 8 are schematically shown the observed frequencies (middle) and the calculated frequencies for model I (top) and model II (bottom). The solid and broken lines indicate the perpendicular and parallel bands, respectively. In the case of model I, the calculated frequencies are in good correspondence to the observed frequencies as shown in Figure 8, and the average errors of model I are 6.11% for the A species and 9.06% for the E_1 species. On the contrary, the calculated frequencies for model II give poor agreement with the observed frequencies, and several calculated modes could not be assigned to any observed bands as shown in Figure 8.

Thus, model I seems to be more reasonable than model II by the over-all considerations on the basis of infrared spectrum and normal coordinate treatment. Furthermore, the potential value of model I is a little lower (3 kcal/mol monomeric unit) than that of model II, though this little difference cannot be said to be significant.

Discussion

In this way two (5/1) helical models, models I and II, have been found reasonable at the early stage of the present work, and one of them, especially model I, has been chosen as the most reasonable one. In Figure 9 the molecular structures of models I and II are shown. In both these models the α-CH_3 group and the side chain ester group are nearly coplanar. The ester groups are packed in the spaces between the turns of the skeletal chain, so that the helical chain becomes compact on the whole. The main difference between model I and model II lies in the internal rotation angles τ_2 which is nearly *cis* (−24°) in model I, and is nearly *trans* (154°) in model II. Model II is similar to the (5/1) helix model reported by Liquori, *et al.*,[4] while model I has not yet been reported.

In this work, the conformational analysis was carried out on the isolated molecular chain, in which the interchain interactions in the crystalline lattice were not taken into account. In general, however, the intrachain interactions seem to play a more important role than the interchain interactions in making the most stable conformation of one molecular chain. In this sense, it may be considered that the molecular structure of isotactic PMMA may be composed of the conformation essentially of model I even in the actual crystal. So far the well-defined fiber diagrams could not be obtained on the samples of isotactic PMMA. Hence, it may be considered that there are some kinds of disorder in the actual crystal, in which each monomeric unit cannot be located in an equivalent environment in a crystallographic sense. It is necessary to find the condition of preparing the highly ordered crystalline samples giving sharp X-ray patterns in order to clarify this interesting problem.

It may be considered that the conformation of the growing molecular chain in the medium of polymerization is closely related to the mechanism of polymerization; penultimate and penpenultimate effects, etc. In these cases the key point may be the spatial relation between the terminal group of the polymer chain and the adding monomer. Recently Yuki, *et al.*,[18,19] found that trityl methacrylate, $CH_2{=}C(CH_3)[COOC(C_6H_5)_3]$, forms a highly isotactic polymer by anionic polymerization and also an isotactic-rich polymer even by radical polymerization. It is not clear whether the molecular conformations in crystalline region and in the medium of polymerization are similar or not. If we assume that poly(trityl methacrylate) takes the helical conformation on the process of polymerization, the bulky trityl group may be favorable to the conformation of model I in the medium rather than that of model II, since the ester CH_3 (or trityl in this case) groups point outward from the helix rather than the case of model II as shown in Figure 9.

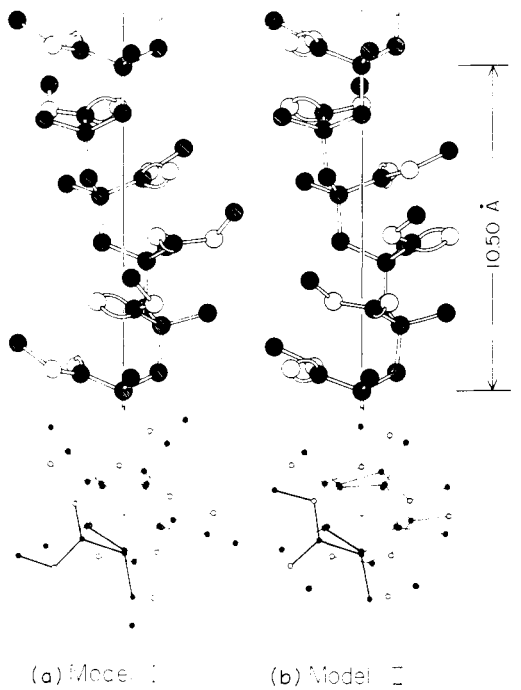

Figure 9. The molecular models of isotactic PMMA: (a) model I, and (b) model II.

Acknowledgments. The authors wish to express their gratitude to Dr. Y. Kotake of the Research Laboratory, Mitsubishi Rayon Co., Ltd., for kindly giving them the highly tactic samples.

(18) H. Yuki, K. Hatada, Y. Kikuchi, and T. Niinomi, *J. Polym. Sci., Part B*, **6**, 753 (1968).
(19) H. Yuki, K. Hatada, T. Niinomi, and Y. Kikuchi, *Polym. J.*, **1**, 36 (1970).